

Perfusion computed tomography for detection of hepatocellular carcinoma in patients with liver cirrhosis

Michael A. Fischer^{1,2} · Nikolaos Kartalis^{1,2} · Aristeidis Grigoriadis^{1,2} · Louiza Loizou^{1,2} · Per Stål³ · Bertil Leidner^{1,2} · Peter Aspelin^{1,2} · Torkel B. Brismar^{1,2}

Received: 16 July 2014 / Revised: 18 March 2015 / Accepted: 23 March 2015 / Published online: 23 April 2015
© European Society of Radiology 2015

Abstract

Purpose To evaluate the diagnostic performance of dynamic perfusion CT (P-CT) for detection of hepatocellular carcinoma (HCC) in the cirrhotic liver.

Materials and methods Twenty-six cirrhotic patients (19 men, aged 69±10 years) with suspicion of HCC prospectively underwent P-CT of the liver using the 4D spiral-mode (100/80 kV; 150/175mAs/rot) of a dual-source system. Two readers assessed: (1) arterial liver-perfusion (ALP), portal-venous liver-perfusion (PLP) and hepatic perfusion-index (HPI) maps alone; and (2) side-by-side with maximum-intensity-projections of arterial time-points (art-MIP) for detection of HCC using histopathology and imaging follow-up as standard of reference. Another reader quantitatively assessed perfusion maps of detected lesions.

Results A total of 48 HCCs in 21/26 (81 %) patients with a mean size of 20±10 mm were detected by histopathology (9/48, 19 %) or imaging follow-up (39/48, 81 %). Detection rates (Reader1/Reader2) of HPI maps and side-by-side analysis of HPI combined with arterial MIP were 92/88 % and 98/96 %, respectively. Positive-predictive values were 63/63 % and 68/71 %, respectively. A cut-off value of ≥85 % HPI and

≥99 % HPI yielded a sensitivity and specificity of 100 %, respectively, for detection of HCC.

Conclusion P-CT shows a high sensitivity for detection of HCC in the cirrhotic liver. Quantitative assessment has the potential to reduce false-positive findings improving the specificity of HCC diagnosis.

Key points

- Visual analysis of perfusion maps shows good sensitivity for detection of HCC.
- Additional assessment of anatomical arterial MIPs further improves detection rates of HCC.
- Quantitative perfusion analysis has the potential to reduce false-positive findings.
- In cirrhotic livers, a hepatic-perfusion-index ≥ 99 % might be specific for HCC.

Keywords Liver cirrhosis · Hepatocellular carcinoma · Perfusion imaging · Computed tomography · Arterialized pseudolesion

Introduction

Hepatocellular carcinoma (HCC) is the most common primary malignancy of the liver and one of the most common cancers worldwide [1]. Liver cirrhosis is the major risk factor for development of HCC, which is predominately caused by alcoholism or chronic infectious disease such as hepatitis B or C [2].

To date, cross-sectional imaging modalities are important clinical tools for establishing the diagnosis of HCC [3]. In patients with liver cirrhosis and/or chronic hepatitis B/C, current guidelines of the American and European Association for the Study of Liver Disease (AASLD /EASLD) allow non-invasively establishment of the diagnosis of HCC if a nodule ≥10 mm exhibits arterial contrast media (CM) uptake

✉ Michael A. Fischer
michaelalexander.fischer@usz.ch

¹ Department of Clinical Science, Intervention and Technology, Division of Medical Imaging and Technology, Karolinska Institute, 14186 Stockholm, Sweden

² Department of Radiology, Karolinska University Hospital, Huddinge, 14186 Stockholm, Sweden

³ Department of Hepatology, Karolinska University Hospital, Huddinge, 14186 Stockholm, Sweden

followed by CM washout in the venous/late phase [4, 5]. However, using multiphase computed tomography (CT), the diagnostic performance of HCC is still reasonably low with an overall sensitivity of 54–87 % [6–8] and a sensitivity of 48–57 % for HCCs of ≤ 20 mm [9], indicating that changes to tumour arterial blood supply in early HCC are subtle and might be missed on standard imaging [10, 11]. Magnetic resonance imaging (MRI) with liver specific CM outperforms CT regarding detection of small lesions < 2 cm [12, 13], however, availability and applicability of MRI are limited.

Dynamic perfusion CT (P-CT) based on the analysis of haemodynamic processes in the liver is increasingly applied in cirrhotic patients for quantitative assessment of tumour blood supply [14]. Evaluation of P-CT is generally based on arterial liver perfusion (ALP) and portal-venous liver perfusion (PLP) maps calculated from time attenuation curves after injection of a highly concentrated contrast media bolus [15]. In contrast to dynamic contrast-enhanced MRI of the liver, which is a technically challenging and still evolving technique, P-CT allows for reliable and absolute quantification of perfusion characteristics [16]. The degree of arterialization has previously been shown to be an important parameter of carcinogenesis in HCC [17]. The arterialization can be visualized in so-called hepatic index (HPI) maps, reflecting the ratio of arterial versus total liver perfusion (ALP/(ALP+PLP)). At the same time P-CT allows reliable depiction of the peak arterial enhancement of HCC, which varies considerably in cirrhotic patients [18], by condensing all arterial time-points to one single maximum-intensity-projection of the arterial phase (art-MIP) [19]. This makes it possible to both qualitatively and quantitatively assess tumour arterialization, which might improve detection of HCC.

Thus, the purpose of this study was to prospectively evaluate the diagnostic performance of P-CT for detection of HCC and to assess perfusion characteristics of HCC in the cirrhotic liver using imaging follow-up and histopathology as the standard of reference.

Materials and methods

Patients

This prospective study was approved by the local ethics committee and written informed consent was obtained from all patients.

Between August 2012 and September 2013, 40 patients (30 men, ten women; mean age 69 ± 10 years) with Child-Pugh class A or B liver cirrhosis and suspicion of HCC due to previous ultrasound (US) findings or history of HCC underwent P-CT examination of the liver for screening of HCC. Histopathological analysis and/or imaging follow-up served as standard of reference.

Exclusion criteria were patient age < 50 years; previous treatment of more than two liver segments; Child-Pugh class C liver cirrhosis; thrombosis in the main portal branches; as well as contrast-enhanced CT-related contraindications (i.e., iodine hypersensitivity to iodinated contrast medium and nephropathy with an estimated glomerular filtration rate of ≤ 30 mL/min).

From all patients undergoing P-CT of the liver, 8/40 (20 %) patients were excluded as no follow-up examination could be performed due to patient's death ($n=3$) or as patients were lost to follow-up examinations ($n=5$), while 5/40 (13 %) patients were excluded due to advanced stage disease, including nodal and/or distant metastases, thus resulting in systemic anti-angiogenic treatment (sorafenib). Finally, 1/40 (3 %) patients was excluded due to technical failure of the CM power injector.

Thus, statistical analysis was conducted in 26 patients (19 men and seven women), with a mean age of 69 ± 10 years; range 50–88 years. Patient demographics are given in Table 1.

Lesion-based reference standard

In 6/26 (23 %) patients, histopathological analysis of resected specimens (partial liver resection, $n=3$; transplantation; $n=2$) and of fine-needle biopsy (FNB; $n=1$) served as standard of reference. Specimens were routinely processed and stained with haematoxylin-eosin. Diagnosis of HCC was made according to the International Working Party criteria [20].

In 24/26 (92 %) patients imaging follow-up with multiphase CT served as standard of reference with a mean follow-up time of 181 ± 75 days (range, 79–310). Diagnostic criteria for HCC were presence of HCC specific imaging

Table 1 Demographic and clinical data of study subjects ($n=26$)

Age, median (range), y	69 (50–88)
Gender male/female, number (%)	19/7 (73 /27)
Aetiology of liver cirrhosis	
HBV positive, number (%)	2 (8)
HCV positive, number (%)	9 (34)
Alcoholic liver disease, number (%)	13 (50)
Non-alcoholic liver disease, number (%)	2 (8)
Barcelona Clinic Liver Cancer (BCLC) stage	
Stage A, number (%)	8 (31)
Stage B, number (%)	18 (69)
No previous treatment	17 (65)
Previous treatment	9 (35)
Partial liver resection, number (%)	1 (11)
Transarterial chemo-embolization, number (%)	8 (90)
One segment, number (%)	4 (44)
Two segments, number (%)	4 (44)

HBV hepatitis B virus, HCV hepatitis C virus

features according to the AASLD and/or EASLD including arterial enhancement with subsequent washout in the portal or late-venous phases [4, 5]. The criteria for benign lesions were a lack of HCC-specific imaging criteria and (a) the lesion decreased in size during imaging follow-up at any time or (b) the lesion remained unchanged in size during follow-up of at least 180 days.

Perfusion CT imaging

All patients were examined with a second-generation 64-slice dual-source CT system (Somatom Definition Flash, Siemens Healthcare, Forchheim, Germany) using the previously described 4D dynamic-spiral-scan mode with variable pitch [15].

The scan volume was individually defined by a supervising radiologist on the topogram in order to cover the entire liver. Scanning was initiated 8 s after contrast media application (Iomeron[®], 400 mg iodine/ml; Bracco Diagnostics Inc., Princeton, NJ, USA) to allow acquisition of baseline non-enhanced images. Each examination was performed in two consecutive breath-holds, allowing the patient to breathe out and back in again after the initial breath-hold at the start of the examination could not be held any longer. Further protocol specifications are given in Table 2. The volume CT dose index ranged from 144 to 162 mGy and the dose-length product (DLP) ranged from 2131 to 3020 mGy×cm, with a mean DLP of 2644 mGy×cm per patient. Using the standard

conversion coefficient for the abdomen ($\kappa=0.015$ mSv/[mGy x cm]) the calculated effective radiation dose of the applied protocol was 32–45 mSv and 40 mSv/patient, respectively [21].

Image post-processing

The volumetric raw data set was reconstructed with a slice thickness of 3 mm and an increment of 1.5 mm, using a medium smooth tissue convolution kernel (B20f). All images were transferred to an external workstation (Multi-Modality Workplace, MMWP, Siemens Healthcare) for further image post-processing using the dedicated perfusion application (Syngo Volume Perfusion CT Body, Siemens). Data processing included automatic motion-correction and noise-reduction of the time-resolved data set. Two image-sets were reconstructed (Figs. 1, 2 and 3):

1. Colour-coded perfusion maps visualizing the arterial liver perfusion (ALP, in mL/min/100 mL), portal-venous perfusion (PVP, in mL/min/100 mL) and hepatic perfusion index (HPI, ALP/ALP+PVP, in %) using the adapted maximum slope method according to Tsushima et al. [22].
2. Maximum intensity projections of the late arterial-phase (art-MIP) containing all arterial time-points of the time-resolved raw data set were retrospectively reconstructed using the time-enhancement curves derived from perfusion analysis to separate the arterial from the portal and portal-venous phases [19].

Enhancement of the liver parenchyma of all perfusion maps was coded in the centre of the scale. All images were transferred to the Picture Archiving and Communication System (PACS) of the institution for review.

Image quality

Image quality (IQ) of all previously mentioned image sets ($n=40$) were evaluated in consensus by two board-certified radiologists (Reader 1 (R1), MA.F. and Reader 2 (R2), N.K. with six and 16 years of experience, respectively), who were blinded to the final diagnosis. All data-sets were ranked from 1–3 according to extent of motion artefacts and delineation of liver lesions as: (1) non-diagnostic, severe artefacts and/or poor delineation of liver lesions; (2) diagnostic, moderate artefacts and/or moderate delineation of liver lesions; and (3) diagnostic, little to no artefacts and/or good to excellent delineation of liver lesions.

Hepatocellular carcinoma (HCC) detection

Perfusion maps and art-MIPs of the 26 patients with valid reference standards were reviewed for detection of HCC by

Table 2 Perfusion CT imaging protocol

Scan parameters	
Scan width (cm)	14.8–18.2
Scan delay (s)	8
No. of scans	30–36
Scan direction	Cranio-caudal alternating
Cycle time (s)	1.5–1.75
Tube voltage (kV)	80/100
Tube current (mAs/rot)	175/125
Slice acquisition (mm)	128×0.6*
Total examination time (s)	54
Contrast material	
Dosage (mL)	60
Iodine concentration (mg/mL)	400
Contrast flow (mL/s)	7
Injection time (s)	8.5
Radiation dose	
Volume CT dose index (mGy)	144–162
Dose length product (mGy×cm)	2131–3020
Effective dose estimation (mSv)	32–45°

*Using the z-flying focal spot

°Conversion factor $k=0.015$ mSv/(mGy x cm)

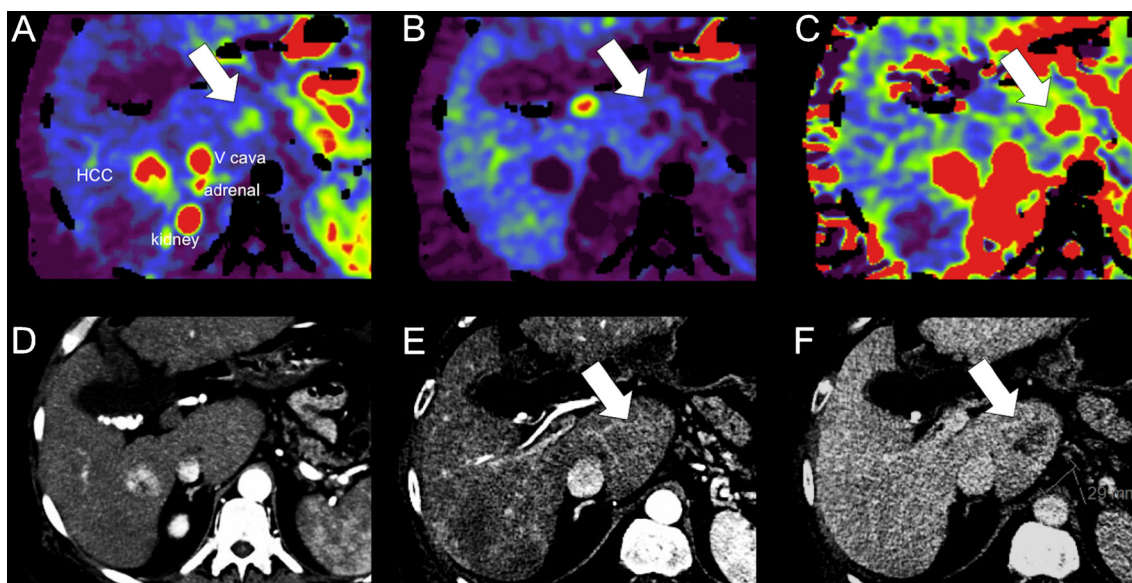


Fig. 1 A 68-year-old man with non-alcoholic steatohepatitis and previously treated hepatocellular carcinoma (HCC) (trans-arterial chemo-embolization) in liver segment VI. Both readers depicted the known HCC in liver segment VI as well as an additional slightly hypervascular lesion in liver segment I (white arrow) on the arterial liver perfusion map (A), portal-venous liver perfusion map (B) and hepatic perfusion index map

(C). The corresponding maximum intensity projection of the arterial phase (D) derived from the time-resolved perfusion series depicted the known HCC in segment VI, whereas the lesion in segment I was not depicted. Follow-up multiphase CT (E, F) after 6 months confirmed the HCC showing a growth of the lesion with slight enhancement in the arterial phase (E) and strong wash-out in the late venous phase (F)

two independent board-certified radiologists (Reader 3 (R3), A.G. and Reader 4 (R4), L.L. with 7 and 8 years of experience, respectively), who were blinded to clinical findings and all other imaging modalities, using a standard PACS

workstation. The perfusion maps, i.e., the ALP, PLP and HPI maps, were assessed separately and prior to presentation of the art-MIP in order to determine the additional value of side-by-side assessment of perfusion maps and art-MIP.

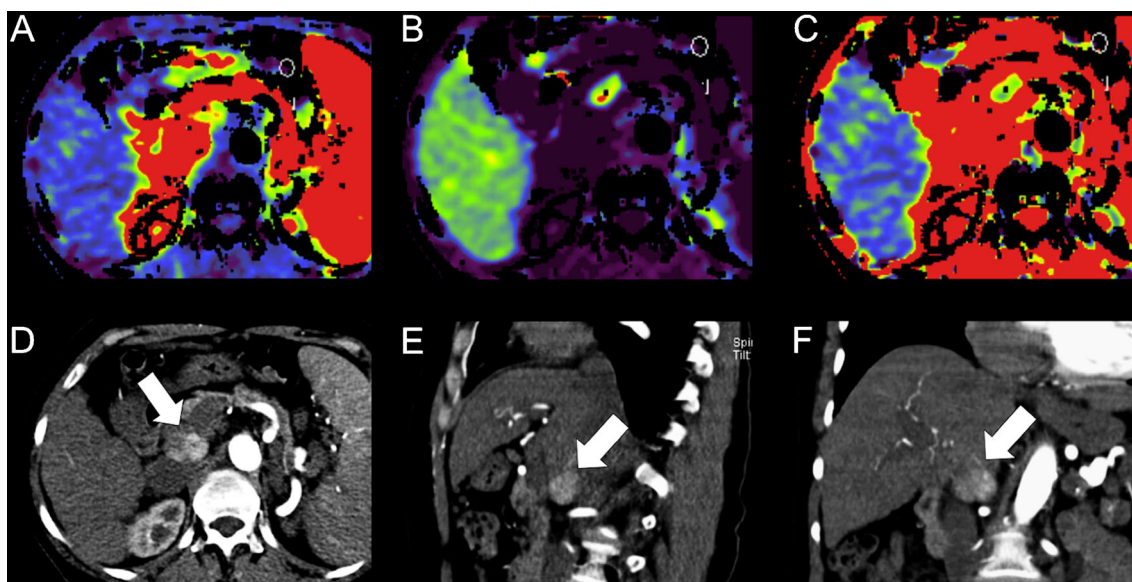


Fig. 2 A 73-year-old woman with hepatitis C-induced liver cirrhosis and three hepatocellular carcinomas (HCCs) diagnosed on surveillance with CT. On the arterial liver perfusion (A), portal-venous liver perfusion (B) and hepatic perfusion index (C) maps the HCC of liver segment I was not depicted by both readers, probably due to its subcapsular location blending into the surrounding hypervascular structures. The corresponding

maximum intensity projection of the arterial phase (D–F) derived from the time-resolved perfusion series nicely depicts the HCC in segment I allowing determination of the exact extension in the axial (D), sagittal (E) and coronal (F) plane. Sagittal and coronal view (panels E and F) are shown for illustrative purposes; only axial images were reviewed in the study

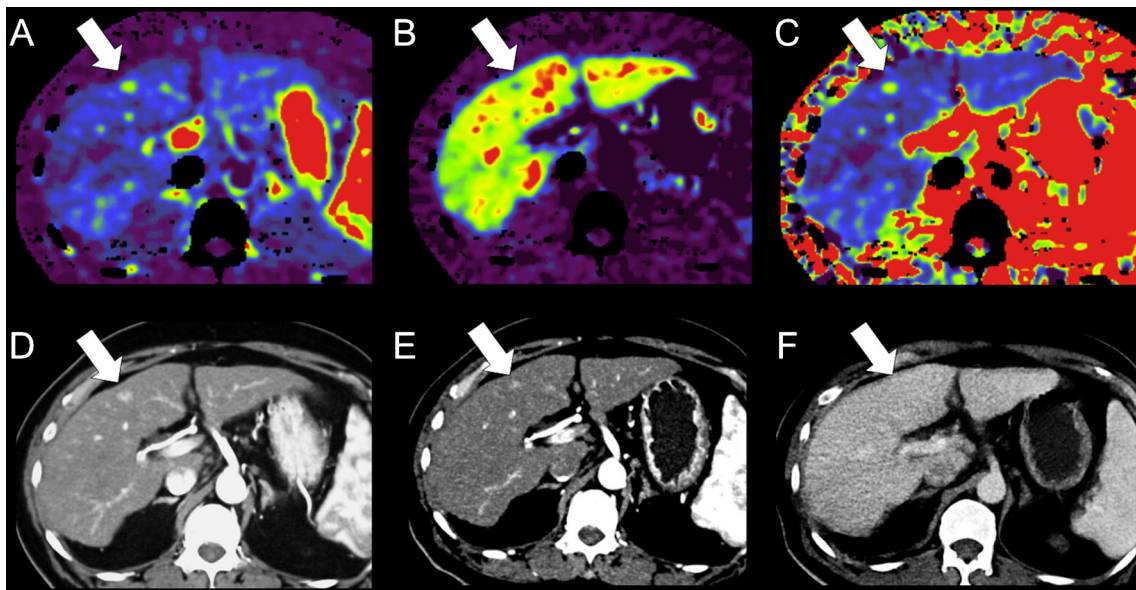


Fig. 3 A 74 year-old man with hepatitis C-induced liver cirrhosis. Arterial liver perfusion map (A), portal-venous liver perfusion map (B) and hepatic perfusion index map (C) as well as the corresponding maximum intensity projection of the arterial phase (D) depicted an arterialized lesion of 12 mm in liver segment IV (white arrow). This lesion was classified as hepatocellular carcinoma by both readers (visual assessment) due to its

nodular shape and increased hepatic perfusion index (HPI) compared to the surrounding liver (C), whereas quantitative assessment of the HPI (84 %) indicated a benign lesion. Follow-up multiphase CT (E, F) after 4 months confirmed the benign nature of the lesion showing a decrease in lesion size in the arterial phase (E) and a lack of wash-out in the venous phase (F)

Both readers recorded the total number (1–10) of liver lesions ≥ 9 mm detected on perfusion maps from cranial to caudal along with the corresponding image number and table position. A lesion qualified as HCC if the lesion was of nodular shape and showed an increased HPI in terms of an increased ALP and/or a decreased PLP compared to the surrounding liver parenchyma. Thereafter the dataset with art-MIPs was reviewed side-by-side with perfusion maps for diagnosis of HCC. A lesion qualified as a HCC if it was nodular in shape and ≥ 9 mm on art-MIP and arterialized (increased HPI) on perfusion maps. If a lesion was not detected on art-MIP nodularity, size was determined on HPI maps. If a lesion was primarily detected on art-MIP, the lesion location and the reason for lesion miss-out on HPI maps, e.g., poor lesion delineation due to adjunct vascular structures, was recorded. Moreover, readers reported on lesions which were exclusively detected on perfusion maps and vice versa.

Perfusion analysis

Perfusion analysis was performed by one of the blinded readers involved in IQ assessment (R1, MA.F.) for all the liver lesions (benign and HCC) using the previously mentioned workstation (Multi-Modality Workplace, MMWP, Siemens Healthcare).

Qualitative assessment Visual grading of ALP and PLP in comparison to the surrounding liver parenchyma was performed for each lesion with elevated HPI using a three-point scale (increased – equal – decreased).

Quantitative assessment For each lesion a circular region of interest (ROI) covering the arterialized lesion (area with increased arterial perfusion) at the level of its greatest transverse diameter without including surrounding normal liver parenchyma was drawn on the HPI map. ROIs placed on the HPI map were automatically copied to the co-registered ALP and PLP maps allowing for assessment of corresponding quantitative perfusion values.

Statistical analyses

The data were descriptively reviewed and statistically tested for normality with the Kolmogorov-Smirnov test. Continuous variables were expressed as means \pm standard deviations. The Wilcoxon-signed rank test was used to test for significant differences between IQ of perfusion maps and art-MIP. The inter-observer agreement for detection of HCC was assessed with κ statistics. Differences between qualitative perfusion analyses were tested with the chi-square test or Mann-Whitney test, respectively, whereas a likelihood-based generalized linear mixed model was used to test for significant differences between quantitative perfusion parameters derived from HCC and benign lesions accounting for the clustering of liver lesions within patients. To investigate the diagnostic accuracy of perfusion parameters for detection of HCC, the area under the curve (AUC) was determined by receiver operating characteristic (ROC) analysis. The cut-off HPI value was chosen to yield 100 % sensitivity and specificity, respectively, for diagnosis of HCC. P-values < 0.05 were considered

statistically significant. All statistical analyses were performed using commercially available software (SPSS, release 17.0, Chicago, IL, USA).

Results

Image quality

IQ of perfusion maps and art-MIPs was diagnostic in all patients. IQ was significantly better for art-MIP (2.9) as compared to perfusion maps (all, $p < 0.01$). Whereas the IQ of ALP (2.5) and PLP (2.4) was similar ($p > 0.05$), delineation of liver lesions was significantly worse on HPI (2.1) maps for both readers (all, $p < 0.01$).

Detection of HCC

Reference standard A total of 83 arterialized lesions in 24/26 (92 %) patients were detected by the reference standard, subdivided into:

- 48/83 (58 %) HCC lesions in 21/26 (81 %) patients; 9/48 (19 %) were histopathologically proven HCCs, while in the remaining 39/48 (81 %) lesions the final diagnosis of HCC was based on multiphase CT imaging follow-up.
- 28/83 (34 %) benign lesions in 16/26 (62 %) patients; 23/28 (82 %) lesions showed a decrease in size at imaging follow-up, while the remaining 5/28 (18 %) lesions showed no change in size over a follow-up period of 6 months.
- 5/83 (6 %) lesions in 3/26 (12 %) patients present on P-CT but were excluded from further analysis due to inconclusive criteria on follow-up imaging, including progress of lesion size but lack of the ‘wash-out’ criteria ($n=3$) and benign imaging criteria with insufficient imaging follow-up interval of less than 180 days ($n=2$).
- 2/83 (2 %) lesions in 2/26 (8 %) patients were present on CT-imaging follow-up but not (even retrospectively) on primary P-CT images. Those lesions were excluded from

further analysis as they probably developed in the time-interval to follow-up imaging.

Thus, 76 arterialized lesions (48 HCC and 28 benign lesions) in 24/26 (92 %) patients underwent statistical analysis.

Diagnostic performance The inter-reader agreement was good for assessment of perfusion maps only (κ , .420) and very good for side-by-side analysis of perfusion maps and art-MIPs (κ , .789).

Perfusion maps and side-by-side analysis detected (R3/R4) a total of 70/67 and 69/65 HCC suspicious lesions (nodular and positive HPI), respectively, with 44/42 and 47/46 true-positive, 26/25 and 22/19 false-positive and 4/6 and 1/2 false-negative findings. Detection rates for HCC (R3/R4) of perfusion maps and side-by-side analysis were 92 % (confidence interval (CI), 82–100) / 88 % (CI, 77–97 %) and 98 % (CI, 92–102 %) / 96 % (CI, 89–102 %), respectively. Positive predictive values (PPV) were 63 % (CI, 50–74) / 63 % (CI, 50–75 %) and 68 % (CI, 56–79 %) / 71 % (CI, 58–82 %), respectively (Table 3). Side-by-side analysis detected significantly more HCCs and showed a significantly higher PPV as compared to perfusion maps for both readers (all, $p < 0.001$). On side-by-side analysis (R3/R4), a total of 2/3 HCCs were additionally detected by art-MIP, whereas 6/6 HCCs were solitarily detected by perfusion maps without a clear correlate on art-MIP.

Perfusion analysis

Mean values of qualitative and quantitative perfusion analysis for HCC ($n=48$) and benign lesions ($n=28$) are displayed in Table 4.

There was no significant difference for visual analysis of ALP and HPI between HCC and benign lesions as compared to surrounding liver parenchyma (all, $p > 0.05$), whereas a significant difference was seen for all quantitative perfusion parameters between HCC and benign lesions (all, $p < 0.001$). Diagnostic accuracy for detection of HCC was excellent for both HPI and PLP, demonstrating an AUC of 0.901 (0.836–

Table 3 Visual assessment of perfusion-CT for detection of hepatocellular carcinoma. Values are given as percentages with corresponding confidence interval (CI) and number (N) of detected lesions in brackets

	Detection rate	Positive predictive value
Perfusion maps alone		
Reader 1	91.6 % (CI, 82–100; N, 44/48)	62.8 % (CI, 50–74; N, 44/70)
Reader 2	87.5 % (CI, 77–97; N, 42/48)	62.6 % (CI, 50–75; N, 42/67)
Side-by-side analysis		
Reader 1	97.9 % (CI, 92–102; N, 47/48)	68.1 % (CI, 56–79; N, 47/69)
Reader 2	95.8 % (CI, 89–102; N, 46/48)	70.7 % (CI, 58–82; N, 46/65)

Note: Perfusion maps included arterial (ALP) and portal-liver perfusion (PLP) maps as well as hepatic index maps (ALP/(ALP+PLP)). Side-by-side analysis included perfusion maps as well as maximum intensity projections of the arterial phase time points reflecting a late arterial phase image

Table 4 Perfusion CT characteristics of detected lesions. Mean values of quantitative analysis as well as X-axis diameter are given with corresponding standard deviation and confidence interval in brackets

	HCC (N=48)	Benign (N=28)	P-value
X-Axis max diameter	20±10 mm (range 9–9)	12±4 mm (range 9–24)	<0.001
Qualitative perfusion analysis			
ALP (Lesion>Liver)	46/48 (95 %)	27/28 (96 %)	>0.05
PLP (Lesion<Liver)	48/48 (100 %)	22/28 (79 %)	<0.01
HPI (Lesion>Liver)	48/48 (100 %)	28/28 (100 %)	>0.05
Quantitative perfusion analysis			
ALP (mL/min/100 mL)	52.6±23.7 (7.2–111.0)	30.4±13.5 (8.6–82.0)	<0.001
PLP (mL/min/100 mL)	1.5±2.3 (0.0–10.9)	11.0±8.6 (1.8–30.0)	<0.001
HPI (%)	95.7±7.5 (65.0–100.0)	73.6±18.6 (44.0–89.6)	<0.001

Note: Qualitative analysis included visual assessment of HCC and benign lesions in comparison to the liver parenchyma

HCC hepatocellular carcinoma, ALP arterial liver perfusion, PLP portal liver perfusion, HPI hepatic index (ALP/ (ALP+PLP))

0.962; $p < 0.001$) and 0.901 (0.838–0.964; $p < 0.001$), respectively, whereas ALP showed an AUC of 0.821 (0.725–0.917; $p < 0.001$; Fig. 4). Sub-analysis of lesions ≤ 25 mm (as no benign lesions > 25 mm were detected) revealed an AUC of 0.923 (0.862–0.984; $p < 0.001$) and 0.915 (0.851–0.979; $p < 0.001$) for HPI and PLP, respectively. A cut-off HPI ≥ 99 % yielded a specificity of 100 % and a sensitivity of 60 %, whereas a cut-off HPI ≥ 85 % yielded a sensitivity of 100 % and a specificity of 36 % for detection of HCC (Fig. 5).

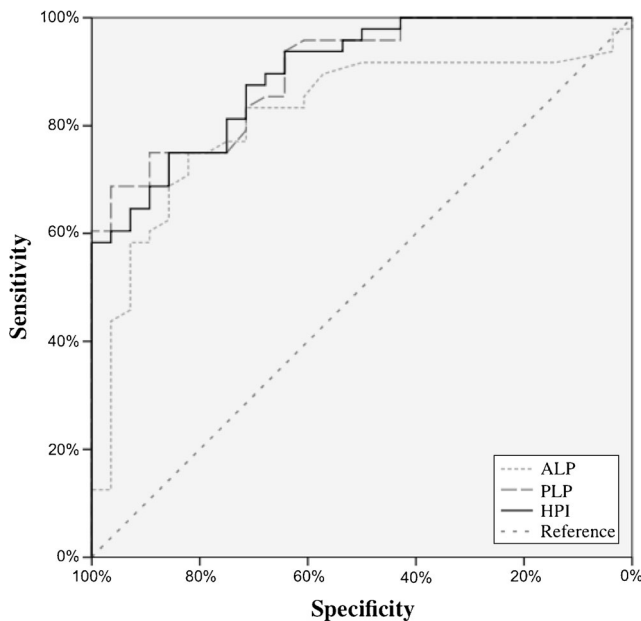


Fig. 4 Receiver operating characteristic (ROC) analysis of arterial liver perfusion (ALP), portal-venous liver perfusion (PLP) and hepatic perfusion index (HPI) for diagnosis of hepatocellular carcinomas (HCCs) in patients with liver cirrhosis. Diagnostic accuracy for detection of HCC was excellent for both HPI and PLP demonstrating an area under the curve (AUC) of 0.901 (0.836–0.962; $p < 0.001$) and 0.901 (0.838–0.964; $p < 0.001$) respectively, whereas ALP showed an AUC of 0.821 (0.725–0.917; $p < 0.001$)

Discussion

To the best of our knowledge this is the first study evaluating the diagnostic performance of perfusion CT for detection of HCC in the cirrhotic liver. Accordingly, we designed a P-CT protocol for screening of HCC providing full liver coverage at a high temporal (< 2 s) and spatial resolution using a double breath-hold regimen to minimize motion artefacts. The latter is of major importance when targeting small nodules in a cirrhotic liver because breathing artefacts can substantially reduce spatial resolution. With our protocol, no major motion artefacts were recorded resulting in a good or excellent diagnostic image quality of the art-MIPs and perfusion maps in all patients. Interestingly, art-MIP showed the best IQ, whereas ALP and PLP maps showed a significantly better depiction of the liver lesions than HPI maps did, which might be due to the high prevalence of intra- and extrahepatic structures with high HPI hampering the delineation of bordering liver lesions on HPI maps (Figs. 1, 2 and 3).

During the carcinogenesis of HCC the vascular supply of the hepatic nodules changes from a mainly portal supply to an exclusively arterial supply [23, 24]. The sensitivity for the detection of early HCC, i.e., less than 2 cm in diameter, at multiphase CT and MRI is poor [25–27], probably due to failure to visualize increased CM uptake during the arterial phase in the cirrhotic liver [25, 28]. By applying a quantitative mapping of the arterial enhancement fraction (AEF) [29] and specific post-processing of the arterial phase [30], the detection rate of HCC can be increased. Similar to the AEF, colour-coded perfusion maps of ALP and PLP reflect the attenuation increment rather than the attenuation itself. Accordingly, our results show an excellent sensitivity of perfusion maps for detection of HCC, superior to the detection rates reported for multiphase CT (48–71 %) [12, 31, 32] and similar to those of angiographic-supported cone-beam CT [31–34]. However, it is important to point out that the HPI map reflects the ratio of

hepatic arterial perfusion to total perfusion. The HPI of a HCC will therefore be elevated if the portal inflow to the tumour is relatively lower than the arterial inflow. Based on the assumption that early HCC loses portal-venous supply before initiation of arterial angiogenesis [35], early HCCs appear bright on HPI maps (ALP/(ALP+PLP)) as ALP>PLP in those lesions. In our material 2/48 (4 %) of the HCCs showed no increased ALP, but a higher HPI than the surrounding liver parenchyma due to a substantial decrease of PLP (Fig. 1). Those lesions might have reflected hypovascular HCC and would have been missed if only ALP maps or art-MIPs had been used for detection.

There was a substantial number of benign lesions with elevated HPI (false-positive findings), resulting in a low positive predictive value (Fig. 4). The majority of these lesions might be explained by arterialized pseudolesions, probably in terms of small arterio-portal shunts, which are increasingly visualized due to the application of a highly concentrated CM bolus [36, 37]. Accordingly, 96 % of benign lesions demonstrated an increased ALP contributing to the increase of HPI, whereas the other 4 % might reflect dysplastic nodules. However, visual P-CT analysis of HPI presents high sensitivity for arterialized lesions in general and further parameters (qualitative or quantitative) are needed to reduce false-positive findings. Side-by-side analysis of perfusion maps and anatomical art-MIPs helped to rule out wedge-shaped arterio-portal shunts, which appeared as false-positive findings on perfusion maps due to the limited morphological information. Interestingly, morphological correlation also increased the sensitivity for detection of HCC. This was because lesions bordering on greater liver vessels, e.g., central portal or liver veins, were occasionally missed when evaluating perfusion maps only (Fig. 2).

In contrast to visual perfusion assessment, quantitative analysis showed a significant difference for all perfusion parameters between HCC and benign lesions (Table 4). Our results on quantitative perfusion values are consistent with previous studies on perfusion of HCC showing an increase in HPI compared to cirrhotic liver parenchyma due to both an increase in ALP and a decrease in PLP. The slightly higher HPI of HCC in our study (96 %) compared to the previous studies (93 %) might be due to differences in the perfusion protocols and ROI placement regimen of the studies [14, 38].

In contrast to previous studies we aimed for discrimination of HCC and benign lesions in the cirrhotic liver, showing an excellent diagnostic accuracy of both HPI and PLP for HCC (Fig. 5). Aiming to reduce false-positive findings of visual perfusion assessment, we determined a cut-off value of $\geq 99\%$ HPI yielding 100 % specificity and a cut-off value of $\geq 85\%$ HPI yielding 100 % sensitivity for diagnosis of HCC. ROC analysis was performed for lesions ≤ 25 mm measured on HPI maps (slight overestimation of size), as arterialized lesions larger than 20 mm on standard imaging should be

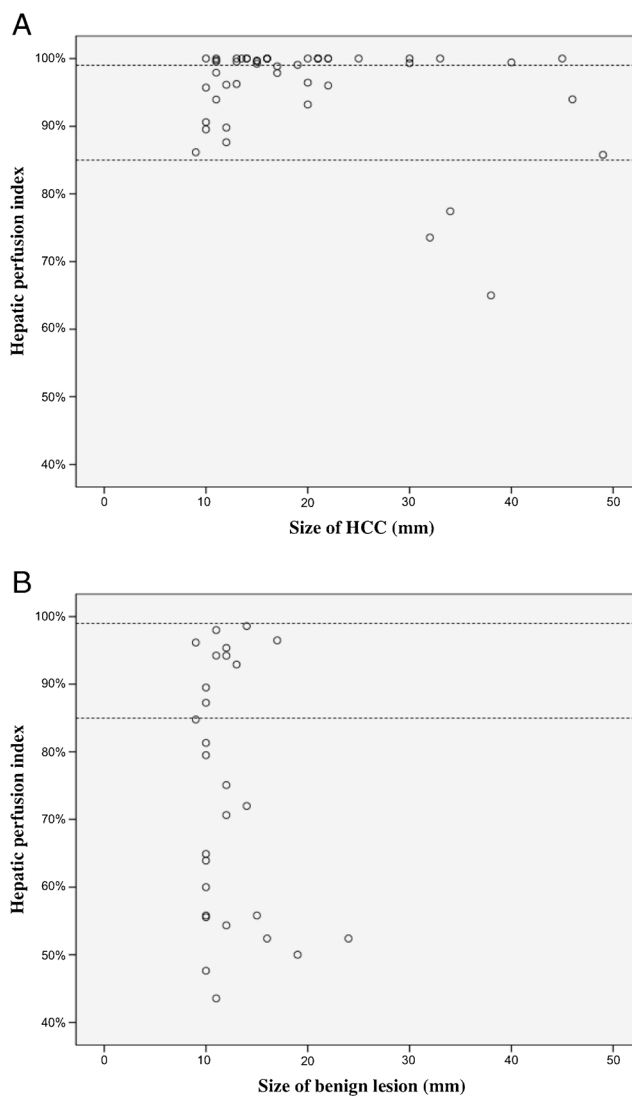


Fig. 5 Hepatic perfusion indices (HPIs) of hepatocellular carcinomas (HCCs) (A) and benign lesions (B) in relation to lesion diameter. All lesions ≥ 25 mm and/or with HPIs $\geq 99\%$ were HCC ($n=33$). All lesions with HPIs $< 85\%$ were benign lesions ($n=18$). By applying these cut-off values to all lesions detected on HPI maps a total of 51/76 (67 %) lesions could have been correctly diagnosed, whereas 25/76 (33 %) lesions including 15/38 (39 %) HCC and 10/28 (36 %) benign lesions would have undergone follow-up to assign final diagnosis

generally regarded as highly suspicious for HCC [28]. By applying this cut-off value a total of 41/66 (62 %) lesions including 23/38 (61 %) HCC and 18/28 (64 %) benign lesions could have been correctly diagnosed, whereas 25/66 (38 %) lesions including 15/38 (39 %) HCC and 10/28 (36 %) benign lesions would have undergone follow-up to assign final diagnosis.

This study has several limitations. First, the study cohort was relatively small and heterogeneous. However, due to the considerable radiation dose, we included only patients with suspicion of HCC and > 50 years of age. Second, no comparison to diagnostic performance of multiphase CT or MRI was

performed due to a great heterogeneity in protocols and time-points of clinically acquired examinations. Third, diagnosis of HCC was confirmed mainly by imaging findings combined with follow-up clinical course without histological verification. Finally, for the P-CT protocol used in this study, the radiation dose (32–45 mSv) was substantial and slightly higher as compared to other studies in the field of whole-liver volume perfusion CT. When using P-CT, there is a trade-off between temporal resolution, image quality and radiation dose. With further refinements of imaging parameters, however, radiation dose might be substantially reduced in future allowing a wider application of P-CT in clinical practice.

We conclude that perfusion CT shows a high sensitivity for detection of HCC in the cirrhotic liver. Quantitative assessment of perfusion parameters has the potential to reduce false-positive findings and correctly diagnose HCC using cut-off values of $\geq 85\%$ and $\geq 99\%$ HPI, respectively.

Acknowledgments The scientific guarantor of this publication is Prof. Peter Aspelin. The authors of this manuscript declare no relationships with any companies whose products or services may be related to the subject matter of the article. The first author was financially supported by the Swiss Radiological Society. No other authors have received any funding. One of the authors has significant statistical expertise. Institutional Review Board approval was obtained. Written informed consent was obtained from all subjects (patients) in this study. No study subjects or cohorts have been previously reported. Methodology: prospective, diagnostic or prognostic study, performed at one institution.

References

- Llovet JM, Burroughs A, Bruix J (2003) Hepatocellular carcinoma. *Lancet* 362:1907–1917
- Schutte K, Bomschein J, Malfertheiner P (2009) Hepatocellular carcinoma: epidemiological trends and risk factors. *Dig Dis* 27:80–92
- Hennedige T, Venkatesh SK (2013) Imaging of hepatocellular carcinoma: diagnosis, staging and treatment monitoring. *Cancer Imaging* 12:530–547
- Bruix J, Sherman M, American Association for the Study of Liver D (2011) Management of hepatocellular carcinoma: an update. *Hepatology* 53:1020–1022
- European Association For The Study Of The L, European Organisation For R, Treatment Of C (2012) EASL-EORTC clinical practice guidelines: management of hepatocellular carcinoma. *J Hepatol* 56:908–943
- Krinsky GA, Lee VS, Theise ND et al (2001) Hepatocellular carcinoma and dysplastic nodules in patients with cirrhosis: prospective diagnosis with MR imaging and explantation correlation. *Radiology* 219:445–454
- Laghi A, Iannaccone R, Rossi P et al (2003) Hepatocellular carcinoma: detection with triple-phase multi-detector row helical CT in patients with chronic hepatitis. *Radiology* 226:543–549
- Monzawa S, Ichikawa T, Nakajima H, Kitanaka Y, Omata K, Araki T (2007) Dynamic CT for detecting small hepatocellular carcinoma: usefulness of delayed phase imaging. *AJR Am J Roentgenol* 188:147–153
- Addley HC, Griffin N, Shaw AS et al (2011) Accuracy of hepatocellular carcinoma detection on multidetector CT in a transplant liver population with explant liver correlation. *Clin Radiol* 66:349–356
- Honda H, Kaneko K, Maeda T et al (1995) Small hepatocellular carcinomas undetected on two-phased incremental computed tomography. Angiographic and clinicopathologic findings. *Invest Radiol* 30:458–465
- Kim I, Kim MJ (2012) Histologic characteristics of hepatocellular carcinomas showing atypical enhancement patterns on 4-phase MDCT examination. *Korean J Radiol* 13:586–593
- Di Martino M, De Filippis G, De Santis A et al (2013) Hepatocellular carcinoma in cirrhotic patients: prospective comparison of US, CT and MR imaging. *Eur Radiol* 23:887–896
- Golfieri R, Renzulli M, Lucidi V, Corcioni B, Trevisani F, Bolondi L (2011) Contribution of the hepatobiliary phase of Gd-EOB-DTPA-enhanced MRI to Dynamic MRI in the detection of hypovascular small (≤ 2 cm) HCC in cirrhosis. *Eur Radiol* 21:1233–1242
- Ippolito D, Capraro C, Casiraghi A, Cestari C, Sironi S (2012) Quantitative assessment of tumour associated neovascularisation in patients with liver cirrhosis and hepatocellular carcinoma: role of dynamic-CT perfusion imaging. *Eur Radiol* 22:803–811
- Goetti R, Leschka S, Desbiolles L et al (2010) Quantitative computed tomography liver perfusion imaging using dynamic spiral scanning with variable pitch: feasibility and initial results in patients with cancer metastases. *Invest Radiol* 45:419–426
- Thng CH, Koh TS, Collins D, Koh DM (2014) Perfusion imaging in liver MRI. *Magn Reson Imaging Clin N Am* 22:417–432
- Inoue T, Hyodo T, Murakami T et al (2013) Hypovascular hepatic nodules showing hypointense on the hepatobiliary-phase image of Gd-EOB-DTPA-enhanced MRI to develop a hypervascular hepatocellular carcinoma: a nationwide retrospective study on their natural course and risk factors. *Dig Dis* 31:472–479
- Ma X, Samir AE, Holalkere NS, Sahani DV (2008) Optimal arterial phase imaging for detection of hypervascular hepatocellular carcinoma determined by continuous image capture on 16-MDCT. *AJR Am J Roentgenol* 191:772–777
- Fischer MA, Leidner B, Kartalis N et al (2014) Time-resolved computed tomography of the liver: retrospective, multi-phase image reconstruction derived from volumetric perfusion imaging. *Eur Radiol* 24:151–161
- International Working P (1995) Terminology of nodular hepatocellular lesions. *Hepatology* 22:983–993
- Bauhs JA, Vrieze TJ, Primak AN, Bruesewitz MR, McCollough CH (2008) CT dosimetry: comparison of measurement techniques and devices. *Radiographics* 28:245–253
- Tsushima Y, Funabasama S, Aoki J, Sanada S, Endo K (2004) Quantitative perfusion map of malignant liver tumors, created from dynamic computed tomography data. *Acad Radiol* 11:215–223
- Hayashi M, Matsui O, Ueda K, Kawamori Y, Gabata T, Kadoya M (2002) Progression to hypervascular hepatocellular carcinoma: correlation with intranodular blood supply evaluated with CT during intraarterial injection of contrast material. *Radiology* 225:143–149
- Park YN, Yang CP, Fernandez GJ, Cubukcu O, Thung SN, Theise ND (1998) Neoangiogenesis and sinusoidal "capillarization" in dysplastic nodules of the liver. *Am J Surg Pathol* 22:656–662
- Fornier A, Vilana R, Ayuso C et al (2008) Diagnosis of hepatic nodules 20 mm or smaller in cirrhosis: Prospective validation of the noninvasive diagnostic criteria for hepatocellular carcinoma. *Hepatology* 47:97–104
- Lauenstein TC, Salman K, Morreira R et al (2007) Gadolinium-enhanced MRI for tumor surveillance before liver transplantation: center-based experience. *AJR Am J Roentgenol* 189:663–670
- Luca A, Caruso S, Milazzo M et al (2010) Multidetector-row computed tomography (MDCT) for the diagnosis of hepatocellular carcinoma in cirrhotic candidates for liver transplantation: prevalence

- of radiological vascular patterns and histological correlation with liver explants. *Eur Radiol* 20:898–907
28. Bolondi L, Gaiani S, Celli N et al (2005) Characterization of small nodules in cirrhosis by assessment of vascularity: the problem of hypovascular hepatocellular carcinoma. *Hepatology* 42:27–34
 29. Kim KW, Lee JM, Klotz E et al (2009) Quantitative CT color mapping of the arterial enhancement fraction of the liver to detect hepatocellular carcinoma. *Radiology* 250:425–434
 30. Bendik E, Noel PB, Munzel D et al (2014) Evaluation of a method for improving the detection of hepatocellular carcinoma. *Eur Radiol* 24:250–255
 31. Zheng J, Li J, Cui X, Ye H, Ye L (2013) Comparison of diagnostic sensitivity of C-arm CT, DSA and CT in detecting small HCC. *Hepatogastroenterology* 60:1509–1512
 32. Pugacheva O, Matsui O, Kozaka K et al (2011) Detection of small hypervascular hepatocellular carcinomas by EASL criteria: comparison with double-phase CT during hepatic arteriography. *Eur J Radiol* 80:e201–e206
 33. Miyayama S, Yamashiro M, Hashimoto M et al (2013) Identification of small hepatocellular carcinoma and tumor-feeding branches with cone-beam CT guidance technology during transcatheter arterial chemoembolization. *J Vasc Interv Radiol* 24:501–508
 34. Kakihara D, Nishie A, Harada N et al (2013) Performance of gadoxetic acid-enhanced MRI for detecting hepatocellular carcinoma in recipients of living-related-liver-transplantation: Comparison with dynamic multidetector row computed tomography and angiography-assisted computed tomography. *J Magn Reson Imaging*. doi:10.1002/jmri.24454
 35. Haaga JR, Haaga R (2013) Acidic lactate sequentially induced lymphogenesis, phlebogenesis, and arteriogenesis (ALPHA) hypothesis: Lactate-triggered glycolytic vasculogenesis that occurs in normoxia or hypoxia and complements the traditional concept of hypoxia-based vasculogenesis. *Surgery* 154:632–637
 36. Ichikawa T, Nakajima H, Nanbu A, Hori M, Araki T (2006) Effect of injection rate of contrast material on CT of hepatocellular carcinoma. *AJR Am J Roentgenol* 186:1413–1418
 37. Irie T, Tsushima Y, Terahata S, Hatsuse K, Kusano S (1996) Influence of liver cirrhosis on pseudolesions in liver at CT during arterial portography. *J Comput Assist Tomogr* 20:914–918
 38. Ippolito D, Fior D, Franzesi CT et al (2014) Tumour-related neoangiogenesis: functional dynamic perfusion computed tomography for diagnosis and treatment efficacy assessment in hepatocellular carcinoma. *Dig Liver Dis* 46:916–922